14th Australasian Fluid Mechanics Conference
Adelaide University, Adelaide, Australia
10-14 December 2001

On the Mechanisms of Wake-Body Interactions in a Tandem Array of Two Square Cylinders

K.L. Lai and M.K. Bull

Department of Mechanical Engineering
University of Adelaide, Adelaide, South Australia, 5005 AUSTRALIA

Abstract

Numerical simulations, by discrete vortex methods, of the flow over a tandem array of two square cylinders when a vortex street is formed within the gap are presented. Attention is concentrated on the interaction between these vortices and the downstream cylinder.

The simulations show that the gap vortices, impinging on the blunt leading edge of the downstream cylinder, undergo distortion and clipping. The minor part of a clipped vortex combines with a separation bubble on a side face of the cylinder to form a secondary vortex.. This vortex, the major part of the clipped vortex, and a further vortex formed by flow separation from the trailing edge of the downstream cylinder are shed, essentially simultaneously, into the wake; they merge to form one of the vortices in the final Karman street downstream of the array. The impingement process couples vortex shedding from the upstream and downstream cylinders, with a phase difference varying linearly with gap width. The calculated fine detail of vortex impingement on the downstream cylinder complements flow-visualisation experiments by other investigators.

Introduction

The numerical simulation of flow over two square cylinders in tandem presented here forms part of a more extensive study of the effects of gaps between bodies and body geometry on the flow over tandem arrays of bluff bodies (of which arrays of thick rectangular plates of rectangular cross-section form one class); detail of flow mechanisms obtainable from numerical simulations is being used to elucidate experimental results.

In the flow over a tandem array of two rectangular plates, shear layers separate from the leading corners of the upstream plate, and generally impinge on the array further downstream. The flow regime established depends on whether impingement occurs on the upstream plate, within the gap between the plates, on the downstream plate, or beyond the downstream plate, and a general classification of the possible flow regimes, on this basis, is given by Bull, Blazewicz and Pickles [1]. In general, the regime depends on the chord-to-thickness ratio of the plates, and varies as a function of the ratio $G = g/h$ of the streamwise length g of the gap between the plates to the plate thickness h.

Numerical simulations, by discrete vortex methods, of the flow over an array of two square cylinders indicate that when the cylinders are separated by a very small gap, $G < 0.5$, the shear layers separating from the leading edges of the upstream cylinder impinge intermittently on the downstream cylinder. The flow intermittently reattaches to a side face of the downstream cylinder and intermittently separates from its trailing edge; a regular vortex street forms behind the array. There is flow through the gap which undergoes periodic reversal, in phase with the vortex shedding cycle. For gaps in the range $0.5<G<2$, the flow is characterised by intermittent reattachment on the downstream cylinder and intermittent separation from both its leading and its trailing edge. A pair of trapped counter-rotating vortices forms in the gap; they oscillate in size at the frequency of vortex shedding of the array. At large gaps, $G > 3$, impingement occurs either on the side faces of the upstream cylinder itself or on the array at a position within the gap; no direct reattachment occurs on the downstream cylinder. A vortex street is formed in the gap; it impinges on the downstream cylinder, and triggers shedding of vortices from it which form the final Karman vortex-street in the wake of the array. In the following sections, the details of the interaction between the vortices in the gap and the downstream cylinder, as revealed by the numerical simulation, are examined.

Numerical Scheme

In a homogeneous incompressible flow, in the absence of external forces, the Navier-Stokes equation in vorticity formulation takes the form

$$\partial_t \omega + \mathbf{u} \bullet \nabla \omega = \omega \bullet \nabla \mathbf{u} + \nu \nabla^2 \omega, \qquad (1)$$

where $\boldsymbol{u}$ is the fluid velocity vector, $\boldsymbol{\omega}=\nabla\times \boldsymbol{u}$ the vorticity, t time and ν the fluid viscosity. Implementation of Eq. (1) in vortex methods for calculating two-dimensional flow involves splitting the motion in each time step into two fractional steps, one of convection of vorticity ($\partial_t\boldsymbol{\omega}+\boldsymbol{u}\cdot\nabla\boldsymbol{\omega}=0$) and one of diffusion ($\partial_t\boldsymbol{\omega}=\nu\nabla^2\boldsymbol{\omega}$) (vortex stretching $\boldsymbol{\omega}\cdot\nabla\boldsymbol{u}$ only being possible in three-dimensional flow). For flow over a system of N solid bodies, each approximated by M_q panels (q=1,2,…N) and with the vorticity distribution in the flow represented by Z discrete vortices with circulations $\Delta\Gamma_j$ (j=1,2,…Z), the boundary condition of zero-velocity on the body surfaces is satisfied by a vortex sheet on the surface of each body. These vortex sheets are approximated by a set of two-dimensional surface-vorticity elements, with strengths $\gamma(s_{qn})$, q=1,2,…N, n=1,2,…M_q, one for each of the panels s_{qn}. Consideration of the boundary condition on all panels of all bodies in the system leads to a set of ΣM_q simultaneous linear equations for the unknown strengths of the elemental vortex sheets $\gamma(s_{qn})$. The condition of zero-circulation, and thus the closure of surface-pressure distribution, on the solid bodies is satisfied by enforcement of the condition $\Sigma\gamma(s_{qn})\Delta s_{qn} = 0$ on each body (where Δs_{qn} is the panel length). The vorticity created at the solid boundaries is shed into the flow as discrete-vortices, one from each panel with a strength of $\gamma(s_{qn})\Delta s_{qn}$. These vortices become part of the set with circulation $\Delta\Gamma_j$, j = 1,2,...Z. The discrete vortices are convected with local flow velocity. Diffusion of vorticity is modelled by the random walk process as proposed by Chorin [4]. Thus modelling of the flow over solid bodies by the method of discrete vortices involves determination of the circulations of the "bound" discrete vortices, and their shedding, convection and diffusion. The evolution of the flow is determined from the solution for the vorticity distribution as a function of space and time, from which the velocity and pressure fields at any general point in the flow domain can be calculated.

Flow Simulations

Simulations of flow over an array of two square cylinders in the regime with a vortex street in the gap have been made for G = 3, 4 and 6, at various Reynolds numbers $Re_h=U_\infty h/\nu$ (where U_∞ is

the free-stream flow velocity). The flow is started impulsively from rest at time (non-dimensional in terms of U_∞ and h) $t = 0$, and its subsequent development calculated, using a timestep $\Delta t = 0.02$, until a fully-developed state is reached. The flow is similar for all three gaps, and the particular case of the $G = 4$ array at $Re_h = 500$ will be used here for identifying the details of it. For the fully-developed flow, the complementary plots of the calculated pressure fields, streamlines and vorticity contours are shown in Figure 1. Vortices can be identified most readily as concentrations of vorticity or pressure contours (independent of the frame of reference), but also as sets of closed streamlines (when stationary) or distorted streamlines (when being convected). It should be recalled that the simulations are for two-dimensional flow. However, although flow over large-chord single plates is three-dimensional at $Re_h \approx 1000$, that over arrays of short-chord plates is not expected to exhibit significant three-dimensionality at Reynolds numbers up to about 500. The results presented complement previous numerical studies such as [5] and extensive experimental results [6,9,10,13,14].

Flow over the Upstream Cylinder

The streamline patterns show the shear layers separated from the upstream cylinder impinging either on the side faces of the upstream cylinder itself or on the gap.

The flow on the upstream cylinder is virtually identical to the flow over a single square cylinder (Okajima [7], Okajima *et al.* [8], Sohankar *et al.*[12]): the separated shear layers reattach to the side surfaces intermittently, alternating with completely detached flow in which there is reversed flow over the side surface. The calculated pressure distribution (not shown here) on the upstream cylinder is very similar to that on a single square cylinder: the base-pressure and mean drag coefficients, $C_{pb1} \approx -1$ and $C_{D1} \approx 1.7$, are comparable to the corresponding values [7,10], $C_{pb} \approx -1.1$ and $C_D \approx 1.8$, for a single square cylinder at $Re_h = 500$.

Interaction of the Vortex Street in the Gap with the Downstream Cylinder

The flow over the downstream cylinder is significantly different from that over a single cylinder, because of the effects of impingement of the vortex street shed from the upstream cylinder. A typical sequence of events in the vortex-street impingement can be seen from $t = 58.6$ onwards (Figure 1). At this time, a vortex (of positive circulation) is impinging on the downstream cylinder, while the next vortex (of negative circulation), shed from the lower side of the upstream cylinder and located about midway along the gap, is being convected towards the downstream cylinder ($t = 58.6, 59.6$). As the vortex approaches the downstream cylinder ($t = 59.6$-61.6), the stagnation point on the leading face of the downstream cylinder takes a position near the lower leading corner, and the flow on the entire lower surface of the cylinder is fully-attached. The attached flow on the leading face sweeps upwards and separates from the upper leading corner, forming a leading-edge-separation bubble on the upper surface. When the incident vortex impinges on the downstream cylinder ($t = 61.6$-63.6), it is distorted and partially clipped by the blunt leading edge. The major portion climbs over the lower leading corner and continues to move along the lower side of the downstream cylinder, while the smaller portion is deflected to the front face where it remains for some time ($t = 63.6$-65.6). Under the influence of the next, approaching, upper (positive) vortex, the stagnation point on the leading edge of the downstream cylinder rapidly shifts upwards to a position near the upper leading corner ($t = 61.6$-63.6), as a result of rapid reversal of flow direction on the leading face. The separated flow on the upper surface then changes to fully-attached flow on the entire surface. The fully-attached flow on the lower face of the downstream cylinder gives way to flow separation at the leading corner and reattachment on the side face; a short leading-edge-separation bubble thus forms on the lower face ($t = 63.6$). As this separation bubble develops, the small vortex on the front face of the cylinder, previously formed by clipping of the impinging vortex, is convected around the lower leading-edge corner and merges with the separation bubble ($t = 65.6, 66.6$) to form a secondary vortex. During the process of impingement, clipping, and secondary vortex formation, flow separation from the lower trailing edge leads to the formation of a trailing-face vortex which grows over times $t = 60.6$ - 63.6. This trailing-face vortex and the secondary vortex on the lower face are shed simultaneously into the wake ($t \approx 67.6$). It appears that generally the shedding of the trailing-face vortex is synchronised with the passage of the major part of the clipped impinging vortex over the trailing edge of the downstream cylinder. The vortical structures associated with the major part of the incident vortex, secondary vortex and trailing-face vortex can be clearly identified in the isobar and vorticity contours ($t \approx 67.6$). These vortices merge ($t = 68.6, 69.6$) as they move downstream, to form a vortex in the final Karman street of the array.

As the next vortex (of positive vorticity) shed from the upstream cylinder impinges on the downstream cylinder ($t = 65.6$), the flow on the leading edge, due to the effect of the following (negative) vortex from the upstream cylinder, again rapidly reverses direction; and the stagnation point shifts from near the upper leading corner to near the lower leading corner ($t = 65.6, 66.6$). As a result, the fully-attached flow on the upper side changes to one separating at the leading corner and accompanied by the formation of a leading-edge-separation bubble; at the same time the flow on the lower side changes from separated flow to fully-attached flow. The separation bubble formed on the upper side combined with the smaller part of the clipped impinging vortex is later shed into the flow ($t = 67.6$) and convected downstream together with the main portion of the incident vortex ($t = 68.6$-69.6). The upper trailing-face vortex formed on the downstream cylinder is also shed into the flow at $t = 67.6$. The incident vortex, secondary vortex and the trailing-face vortex merge during downstream convection to form a wake vortex ($t = 69.6$). While the formation and shedding of the secondary vortex and upper trailing-face vortex are taking place, a vortex (of negative vorticity) shed from the lower side of the upstream cylinder is approaching the leading face of the downstream cylinder. The impingement cycle is then repeated. However, the calculations indicate that the impingement cycle is not exactly repeated each time. Successive vortices are not identical, but vary in strength, spatial scale, and regularity of shedding from the upstream cylinder, and do not follow identical paths. The degree of distortion and redistribution of the incident vortical structure which occurs on impingement on the downstream blunt edge is primarily determined by the spatial scale of the vortex and the extent to which its trajectory is laterally offset from the side face of the downstream cylinder. Significant differences in these parameters from one impingement to another can be seen by comparing the vorticity patterns of the impingements at $t = 62.6$ and $t = 68.6$. Consequently, the proportion of the incident vortex clipped by the downstream blunt edge varies, and so does the intensity of the secondary vortex. Irregularities of this type in the vortex-impingement pattern are also observed experimentally (Tang and Rockwell [13]).

Vortex formation on the trailing face of the downstream cylinder is also affected by variations in the scale and lateral offset of the impinging vortices. Consequently, the irregularities in the impingement flow give rise to irregularity in the final vortex street downstream of the array. There are indications that the trailing-face vortices on the downstream cylinder are formed mainly by rolling up of the shear layers separating from the trailing edges (as, for example, in the formation of the lower

trailing-face vortex at $t = 60.6$), but there are also occasions when a side-face vortex convected past the trailing corner becomes the seed of a trailing-face vortex (as in the formation of the upper trailing-face vortex at $t = 61.6$); it appears that both processes make a contribution. However, despite the variations in the vortex-impingement patterns, trailing-face vortex formation is always coupled with vortex impingement and the associated shedding of the secondary vortex. The onset of impingement of a vortex on the downstream cylinder is therefore closely associated with the shedding of a vortex of the opposite sign (formed from the previous impingement) from the cylinder into the wake. It is also closely associated with the shedding of a vortex of opposite sign from the upstream cylinder. Thus, vortices of the same sign are shed from corresponding corners of the upstream and downstream cylinders, at times close to that at which a convected vortex in the gap, of the opposite sign, arrives at the downstream cylinder.

Calculated time-histories of the drag and lift coefficients on the array (not shown here) indicate that, when the flow becomes fully-developed, typically at $t \geqslant 15$, the pressure forces on the cylinders vary periodically with time at the vortex-shedding frequency, but with a phase difference depending on G. As indicated above, the flow over the upstream cylinder is very similar to that over an isolated cylinder. This conclusion is reinforced by the insensitivity to the value of G of the Strouhal numbers determined from lift fluctuations ($St = 0.12$, 0.125 and 0.13 for $G = 3$, 4 and 6 respectively) and their similarity to the value for an isolated square cylinder ($St = 0.132$ at $Re_h = 500$). This suggests that vortex shedding from the upstream cylinder is essentially uninfluenced by the presence of the downstream cylinder when $G \geq 3$. In that case, the phase difference between lift fluctuations on the two cylinders should be proportional to the time taken for vortices shed from the upstream cylinder to traverse the gap, and should vary linearly with G, as found experimentally by Sakamoto, Haniu and Obata [11]. Calculated values for the phase lag (incremented by 2π for consistency with those of Sakamoto *et al.)* are 2.06π, 2.2π and 3.05π for $G = 3$, 4 and 6 respectively; they agree quite well with the empirical experimental linear relation obtained in [11], closely expressible as $(1 + G/3)\pi$. Thus, in the case of $G = 3$, impingement of a vortex on the downstream cylinder is synchronised with simultaneous shedding of vortices of the opposite sign from both upstream and downstream cylinders, while for $G = 6$ impingement is synchronised with shedding of a vortex of the same sign as the impinging vortex from the upstream cylinder and one of the opposite sign from the downstream cylinder.

As a result of vortex-street impingement, the distribution of mean pressure on the downstream cylinder deviates from that on a single cylinder. Most noticeable is the reduced pressure on the leading face ($C_p = 0.1$ for $G = 3$), although this increases with increasing G (to $C_p = 0.7$ at $G = 6$). With increasing G, although the downstream cylinder is still subject to vortex impingement, the overall pressure distribution on it approaches that on the upstream cylinder, and both approach the pressure distribution on a single square cylinder. Vortex impingement also causes the pressure fluctuations to be significantly greater on the downstream than on the upstream cylinder. In accord with experimental findings [2,3], the calculated pressure fluctuations are greatest near the leading edges of the downstream cylinder.

Concluding Remarks

Numerical simulations of the flow over tandem arrays of two square cylinders, with gap widths, $G > 3$, sufficiently large to allow a vortex street to be formed within the gap, have been presented. They show that, for such gaps, the flow over the upstream cylinder - and in particular vortex shedding from it - is insensitive to the presence of the downstream cylinder. Vortex shedding from the downstream cylinder is triggered by impingement on it of the vortices shed from the upstream cylinder. There is therefore a phase difference between the two shedding processes that varies linearly with gap length and is determined by the time taken for vortices shed from the upstream cylinder to traverse the gap between the cylinders. The simulations adequately predict the phase lag, which can be closely represented empirically by $(1+G/3)\pi$

The simulations indicate that the interaction between an impinging vortex and the downstream cylinder follows an intricate sequence of events. The sequence involves clipping of impinging vortices, formation of separation bubbles on the side faces of the cylinder, merging of the minor parts of clipped vortices and separation bubbles to form secondary vortices, formation of trailing-face vortices, and the shedding and subsequent amalgamation of the major parts of clipped vortices, secondary vortices and trailing-face vortices to form the final Karman vortex-street downstream of the array.

References

[1] Bull, M.K., Blazewicz, A.M. and Pickles, J.M. Acoustic radiation from a tandem two-plate array in a fluid flow: dependence on array geometry and flow regime. *Proc.Fifth International Congress on Sound and Vibration, Adelaide, South Australia,* 1997.

[2] Bull, M.K. and Pickles, J.M. (1991). Noise generation mechanisms in the interaction between a vortex wake and a bluff body. *Proc.Int. Conf. on Noise Control Eng. (Inter-Noise 91), Sydney, Australia,* 1991, 403-406.

[3] Bull, M.K., Pickles, J.M. and Li, Y. On vortex-wake/bluff body interactions and noise from circular saws. *Proc. 14th Int. Congress on Acoustics, Beijing, China,* 1992.

[4] Chorin, A.J. Numerical study of slightly viscous flow. *J. Fluid Mech*., **57**, 1973, 785-796.

[5] Kaya, M.O., Kaykayoglu, C.R., Bayar, K.C. and Graham, J.M.R. Numerical simulation of vortex street-edge interaction. *AGARD Conf. Proc.* **494**, 1991, 32-1 –32-12.

[6] Kaykayoglu, C.R. and Rockwell, D. Vortices incident upon a leading-edge: instantaneous pressure fields, *J. Fluid Mech*., **156**, 1985, 439-461.

[7] Okajima, A. Strouhal numbers of rectangular cylinders. *J. Fluid Mech.,* **123**, 1982, 379-398.

[8] Okajima, A., Ueno, H. and Sakai, H. Numerical simulation of laminar and turbulent flows around rectangular cylinders. *Int. J. Num. Methods in Fluids*, **15**, 1992, 999-1012.

[9] Rockwell, D. and Knisely, G. The organised nature of flow impingement upon a corner, *J. Fluid Mech*., **93**, 1979, 413-432.

[10] Rockwell, D., Kaykayoglu, C.R., Sohn, D. and Kuo, C.H. An assessment of some vorticity field-leading edge interactions. In *Shear flow-structure phenomena,*editors A Akay and M. Reischman, *ASME NCA*, **1**, 1985, 79-88.

[11] Sakamoto, H., Haniu, H. and Obata, Y. Fluctuating forces acting on two prisms in a tandem arrangement. *J.Wind Eng.and Ind. Aerod.* **26**, 1987, 85-103.

[12] Sohankar, A, Davidson, L. and Norberg, C. Numerical simulation of unsteady flow around a square two-dimensional cylinder. *Proc.Twelfth Australasian Fluid Mechanics Conference, Sydney, Australia*, 1995, 517-520.

[13] Tang, Y. P. and Rockwell, D. Instantaneous pressure fields at a corner associated with vortex impingement. *J.Fliuds Eng.*,**126**, 1983, 187-204.

[14] Ziada, S. and Rockwell, D. Vortex-leading edge interaction. *J Fluid Mech.,* **118**, 1982,79-107.

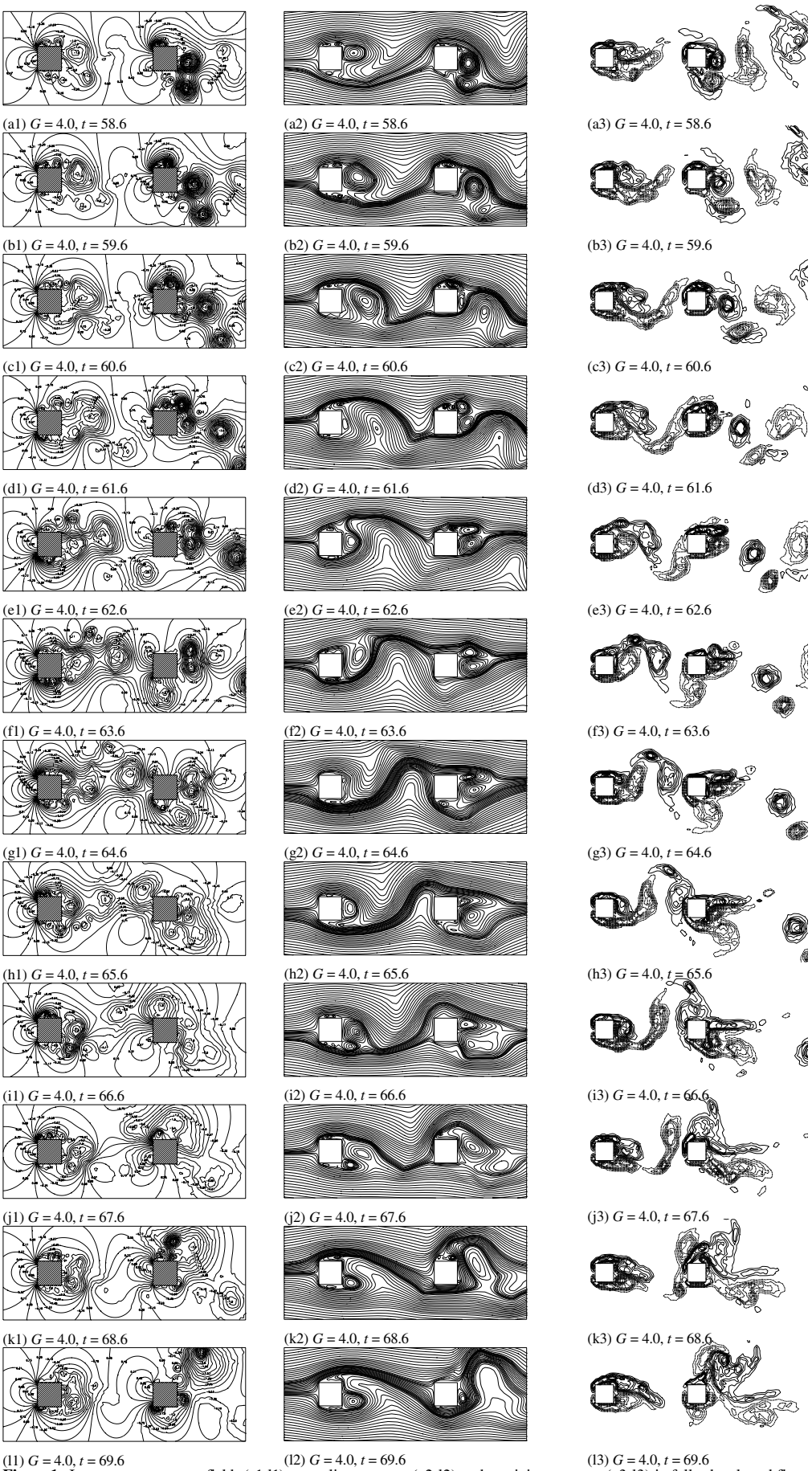

Figure 1. Instantaneous pressure fields (a1-l1), streamline patterns (a2-l2) and vorticity contours (a3-l3) in fully-developed flow over the ($C1 = 1$, $C2 = 1$, $G = 4.0$) array. Numbers shown are coefficients of static pressure. Solid (dashed) lines in vorticity contours represent positive (negative) vorticity.